Supporting information

Economical 550 V energy harvesting from plastic and electronic wastes using human motions

Man Singh[a], Sameer Kumar[a], Alankar Kafle[a], Kalpana Garg[a], Parimal Sharma[b], C. C. Reddy[b] and Tharamani C. Nagaiah[a]*

[a]*Department of Chemistry, Indian Institute of Technology Ropar, Rupnagar-140001, Punjab;*
[b]*Department of Electrical Engineering, Indian Institute of Technology Ropar, Rupnagar-140001, Punjab,*
Corresponding author: Tharamani C. Nagaiah; E-mail: tharamani@iitrpr.ac.in

Materials

Kapton tape (bought from local market), damaged electric wires of old UPS, plastic sheets (obtained from discarded document folder), Vulcan carbon (VC XC-72), copper sulfate pentahydrate ($CuSO_4.5H_2O$, from Chemlabs), sodium sulfate (Na_2SO_4, from Loba Chemie), sulfuric acid (H_2SO_4, from Loba Chemie), polyvinylidene fluoride (PVDF, from Sigma Aldrich), N-methyl pyrrolidinone (NMP, from Sigma Aldrich), acetone (from Spectrochem), deionized water (resistivity > 12 MΩ cm^{-1}) obtained from a Millipore system.

Characterization of materials

Power X-ray diffraction (PXRD) patterns were recorded to analyze the structures of plastic, paper, and electrodeposited samples (e-Cu@plastic and e-Cu@paper). Measurements were performed by using PANanalytical X'PERT pro diffractometer with Cu K_α radiation (λ = 0.1542 nm) in the range 5 to 80˚ at 2˚ min^{-1} scan speed and 0.2 deg step size. Fourier transform infrared (FT-IR) spectroscopy was employed to interpret the presence of heteroatom functionalities in the plastic materials by using a BRUKER TENSOR-II spectrometer in the frequency range 600-4000 cm^{-1} with a spectral resolution of 4 cm^{-1} and 100 scans. Field emission scanning electron microscopy (FESEM), electron-dispersive X-ray spectroscopy (EDX) and elemental dot mapping images were taken to analyze the surface morphology and elemental distribution in e-Cu@plastic and e-Cu@paper sheets using JEOL JSM-7610F FEG-SEM.

Experimental data and results

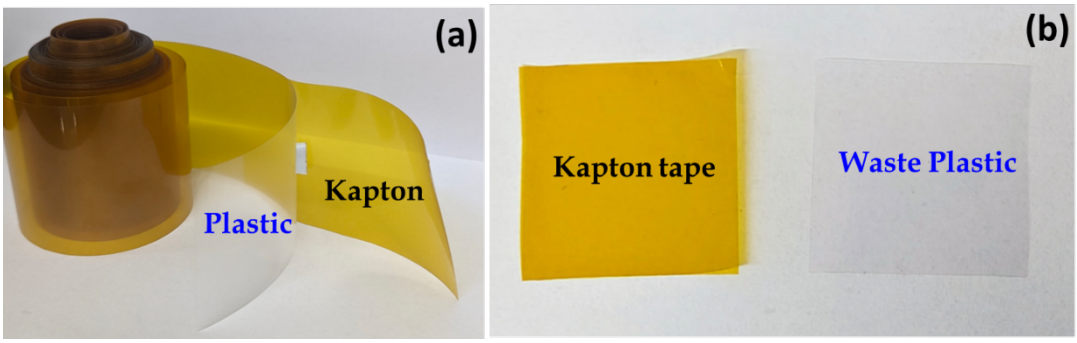

Figure S1. (a) Roll of commercial Kapton tape, (b) pieces of Kapton tape and leftover waste plastic.

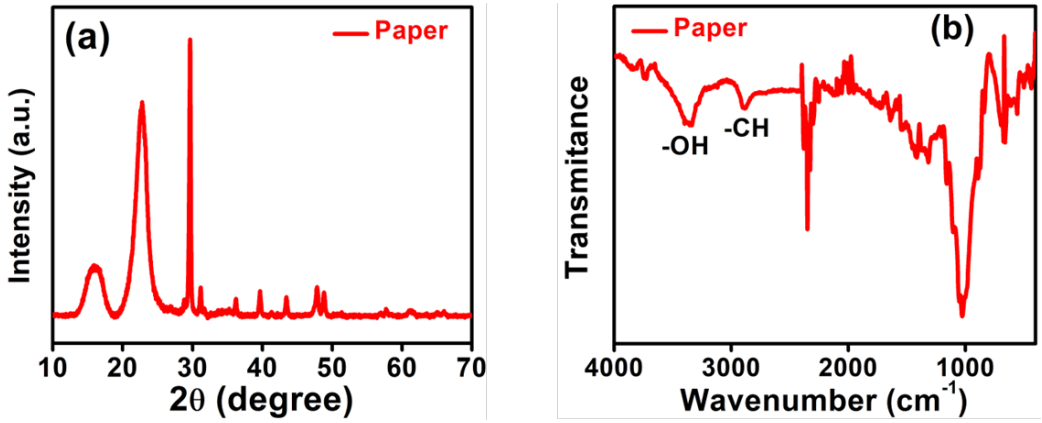

Figure S2. (a) X-ray diffraction pattern, (b) FT-IR spectra of A4 sheet paper.

The FT-IR spectra of paper consist of an absorption band at ~3328 cm^{-1} due to the presence of hydroxyl groups (-OH) and the band at ~2895 cm^{-1} corresponds to the stretching and deformation vibrations of the C-H group in the glucose unit of cellulose.[1] These functional

groups are responsible for the electron-donating nature of paper and thus they can be used as tribo-positive material.

The substrate preparation for the electrodeposition of Cu layer on plastic and paper involved the initial step of carbon coating by conducting carbon slurry (Vulcan carbon XC-72) on single side (Figures S3 & S4). The carbon coating was confirmed by FESEM images, elemental dot mapping and EDX spectra (Figures S5 & S6). Thereafter, the carbon-coated sides were deposited with copper layers via the electrodeposition method. The electrodeposition setup (Figure 1d) involved the use of a direct current (DC) power source with an application of 1.5 V in 0.05 M $CuSO_4$ aqueous solution. The carbon-coated plastic and paper substrates were connected to the cathode (-ve electrode) and a bundle of copper wires recovered from electronic waste of old UPS (uninterrupted power supply) cables were used as the sacrificial anode (Figure S7).

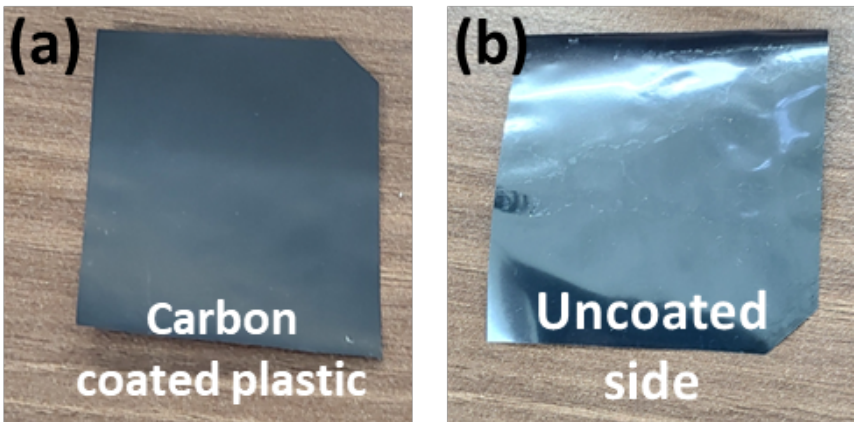

Figure S3. Digital images of (a) carbon coated and (b) uncoated side of waste plastic.

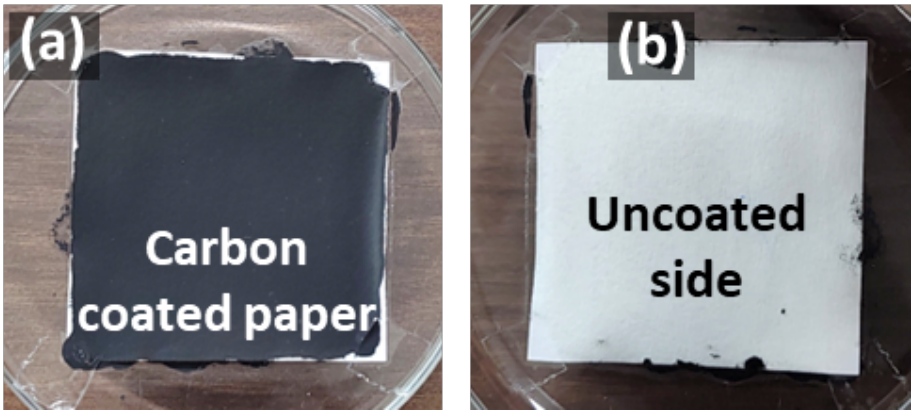

Figure S4. Digital images of (a) carbon-coated and (b) uncoated side of paper.

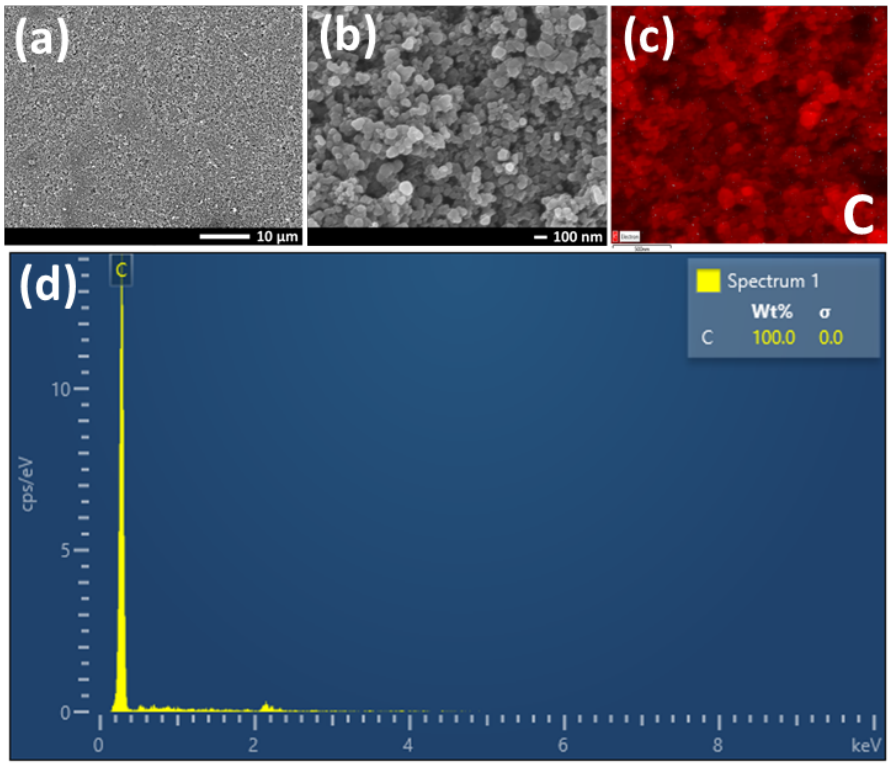

Figure S5. FESEM image of (a-b) carbon-coated plastic. (c) elemental dot mapping image, (d) EDX spectra of carbon-coated plastic.

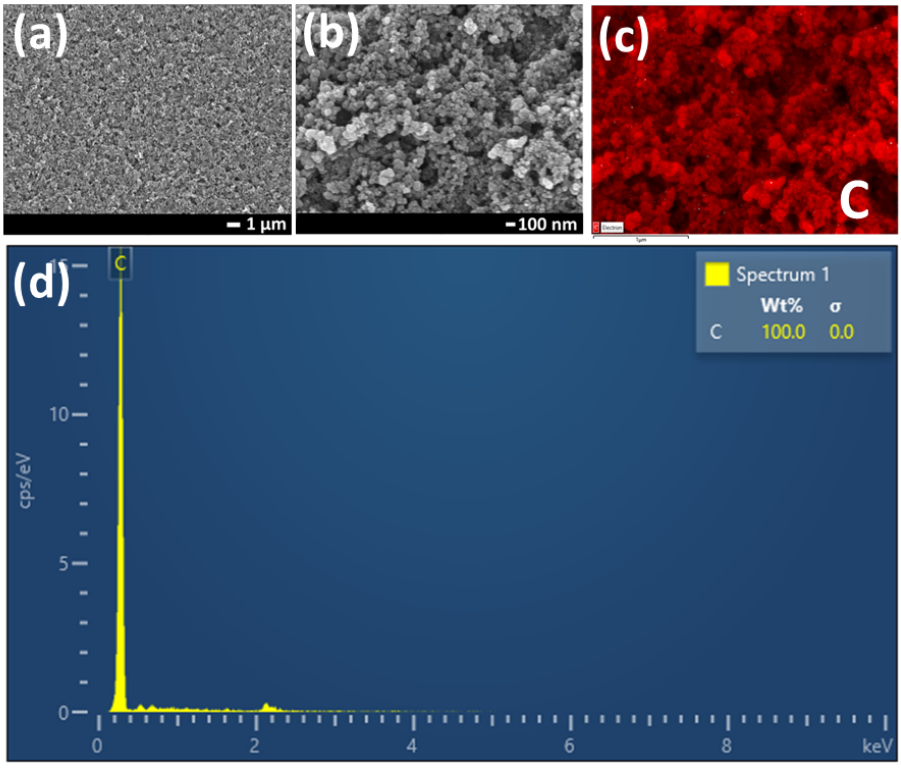

Figure S6. FESEM image of (a-b) carbon-coated paper. (c) elemental dot mapping image, (d) EDX spectra of carbon-coated paper.

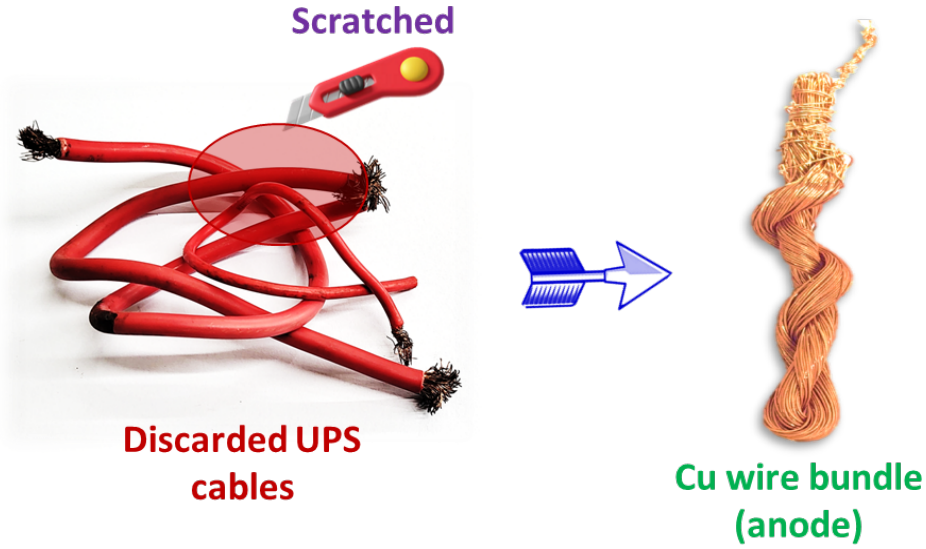

Figure S7. Pictorial representation of Cu wires recovered from electronic waste of discarded UPS cables.

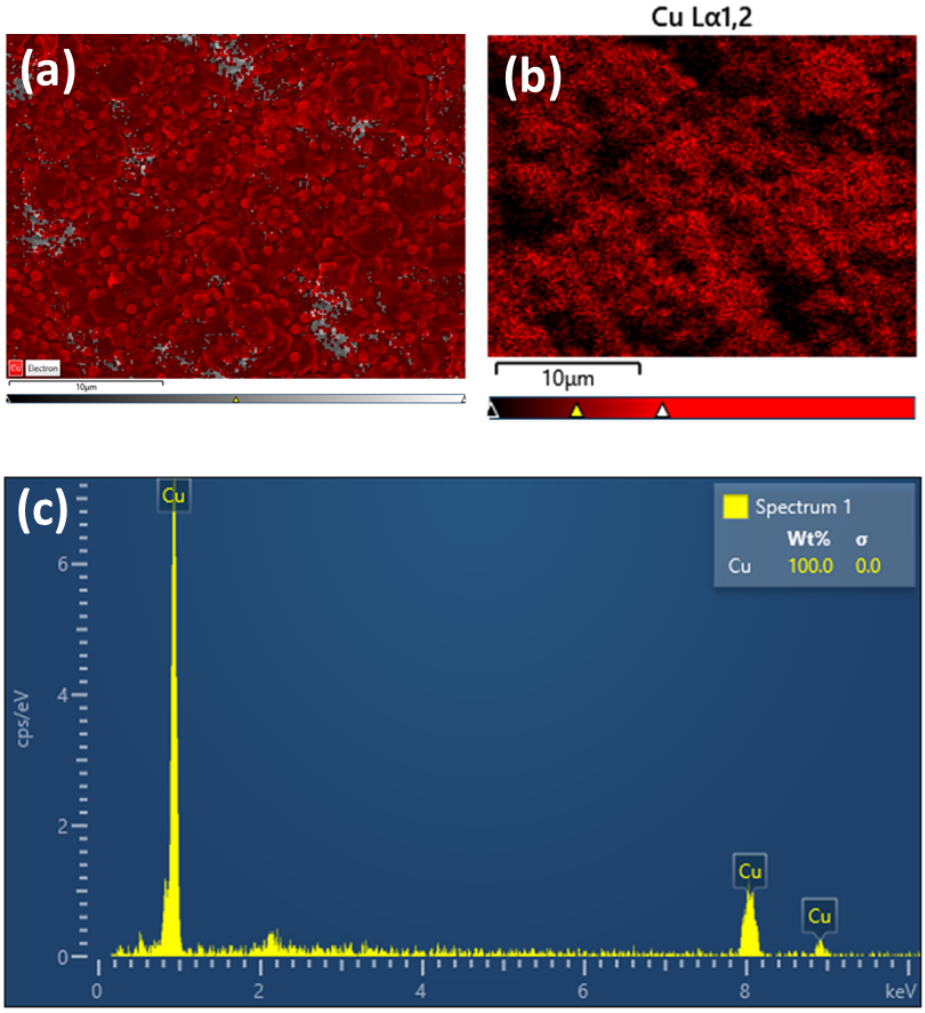

Figure S8. (a) & (b) Elemental dot mapping images, (c) EDX spectra of e-Cu@plastic.

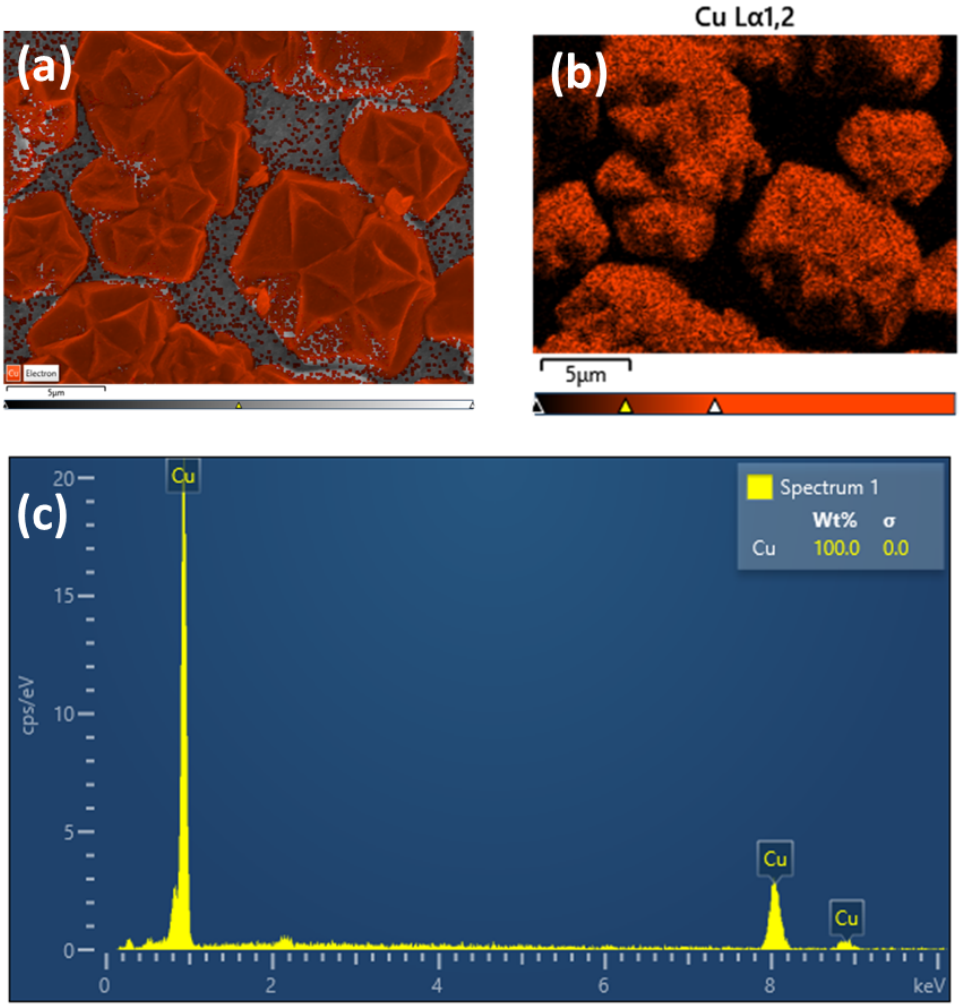

Figure S9. (a) & (b) Elemental dot mapping images, (c) EDX spectra of e-Cu@paper.

Interestingly, electrodeposited Cu on plastic and paper substrates showed different morphologies (Figure 2 (c), (e) & Figure S8-S9). Cu deposited on plastic exhibited the hexagonal morphology with particle dimension in the typical nanometre scale whereas on paper substrate comparatively bigger Cu particles with star-shaped morphology were obtained. The most probable reason for this different morphologies could be the characteristic differences of substrate material. Paper has a porous cellulose network which allows the better anchoring of carbon slurry and thus faster growth during the electrodeposition resulting in the bigger particle size. Whereas, the plastic sheet does not have such porous structure, therefore, resulting in the slower growth and smaller particle size.

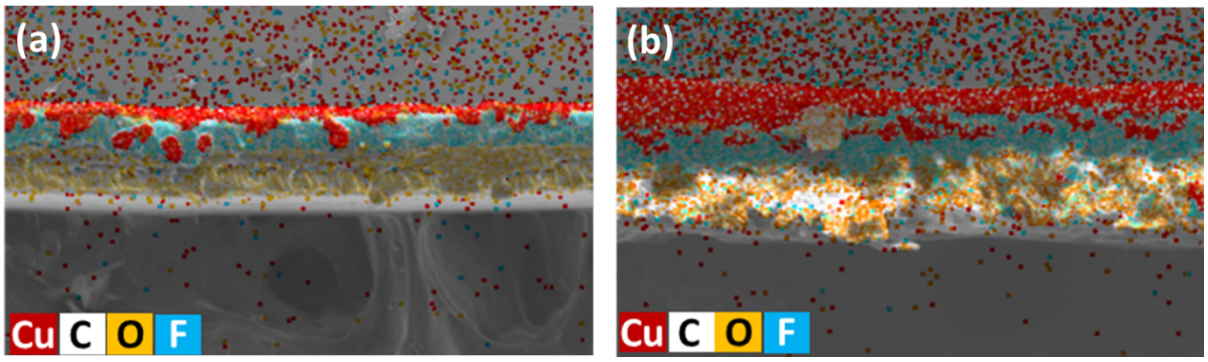

Figure S10. (a) Elemental dot mapping image for the cross-sectional view of (a) e-Cu@plastic and (b) e-Cu@paper.

The cross-sectional elemental dot mapping of e-Cu@plastic (Figure S10a) and e-Cu@paper (Figure S10b) clearly shows the clear distinction of elemental distribution in three layers. Top layer in both the materials shows the presence of electrodeposited Cu. Middle layer shows the presence of carbon along with fluorine representing the carbon layer with PVDF (Polyvinylidene fluoride) binder. Bottom layers (triboelectric layers) show the presence of C and O elements in the PET structure of plastic and cellulose papers.

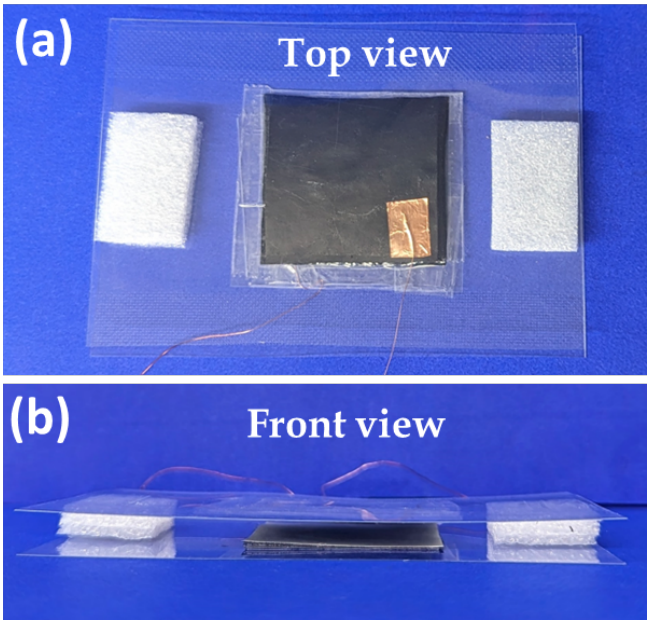

Figure S11. (a) Top view and (b) front view of assembled C@WPP-TENG.

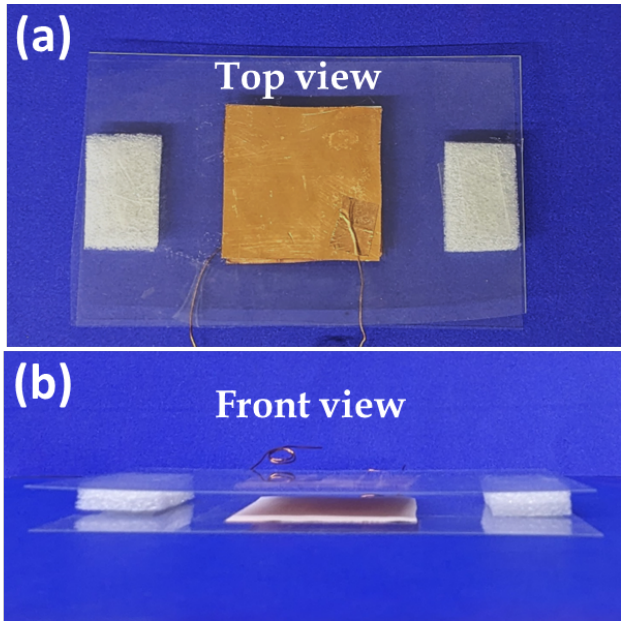

Figure S12. (a) Top view and (b) front view of assembled Cu-tape@WPP-TENG.

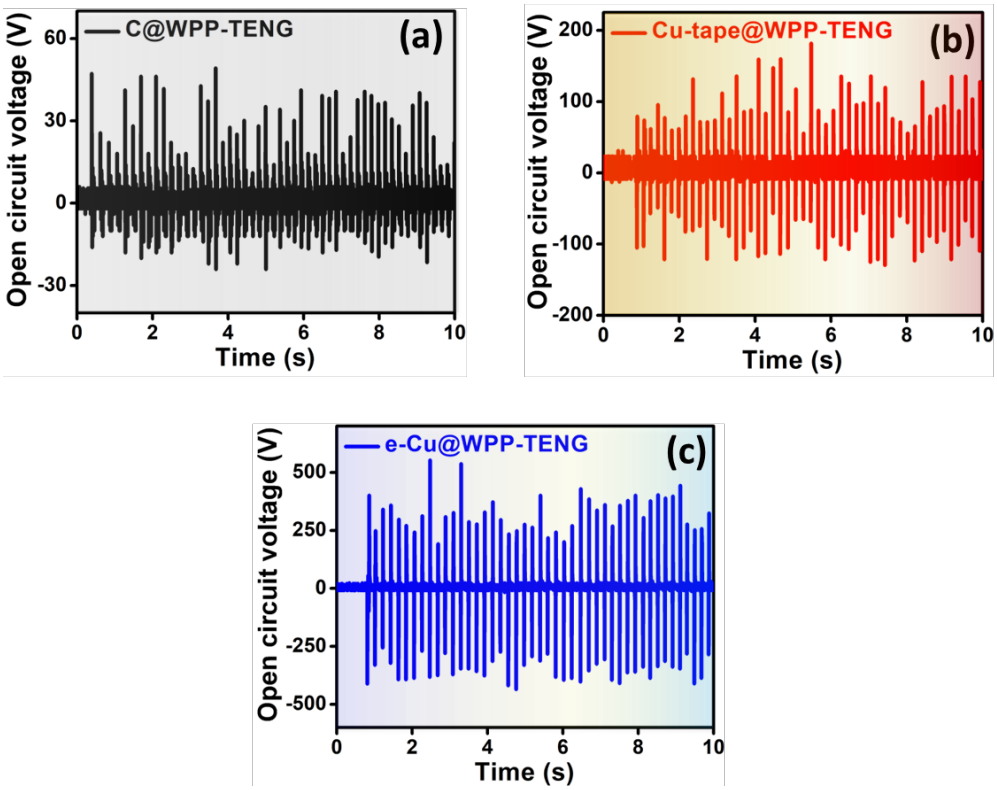

Figure S13. Open-circuit voltages of (a) C@WPP-TENG, (b) Cu-tape@WPP-TENG, (c) e-Cu@WPP-TENG under human hand tapping.

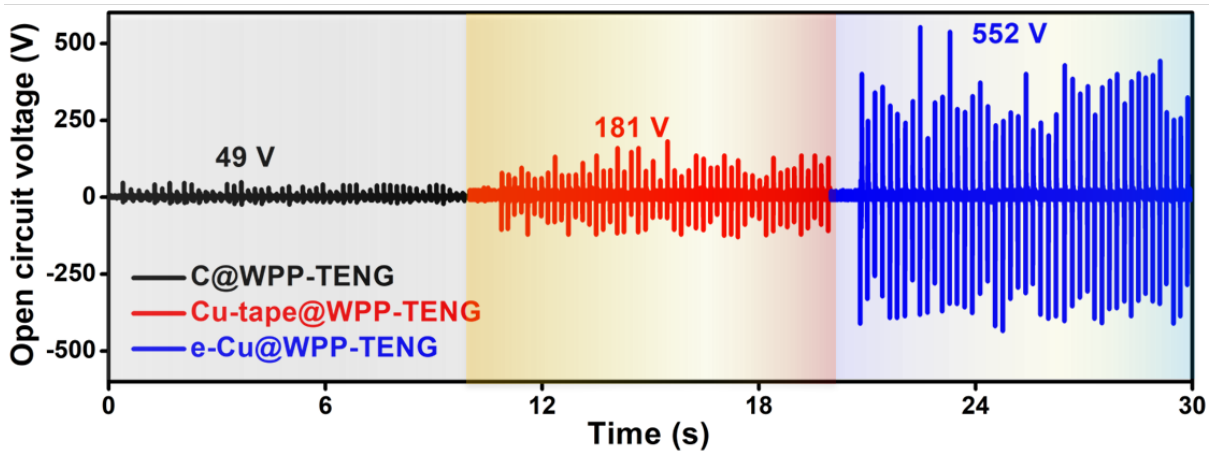

Figure S14. Comparison of open-circuit voltages of (a) C@WPP-TENG, (b) Cu-tape@WPP-TENG, (c) e-Cu@WPP-TENG under human hand tapping.

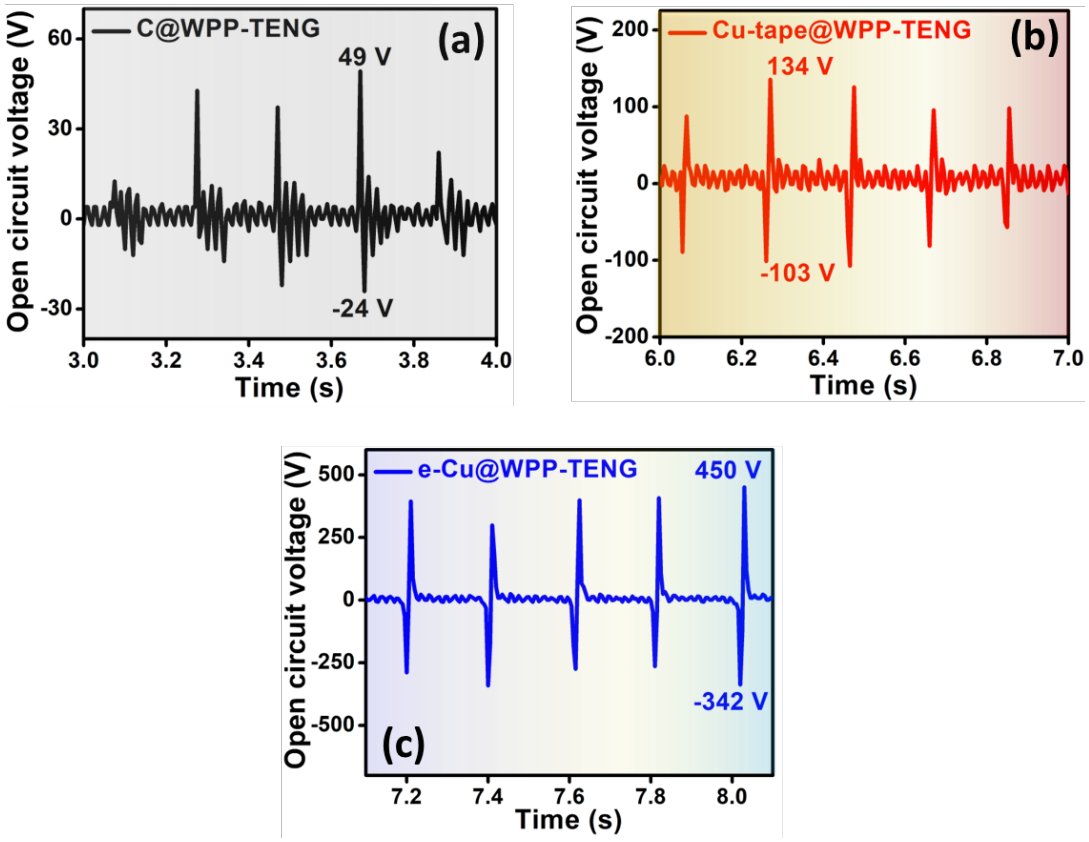

Figure S15. Open-circuit voltages of (a) C@WPP-TENG, (b) Cu-tape@WPP-TENG and (c) e-Cu@WPP-TENG under hand tapping.

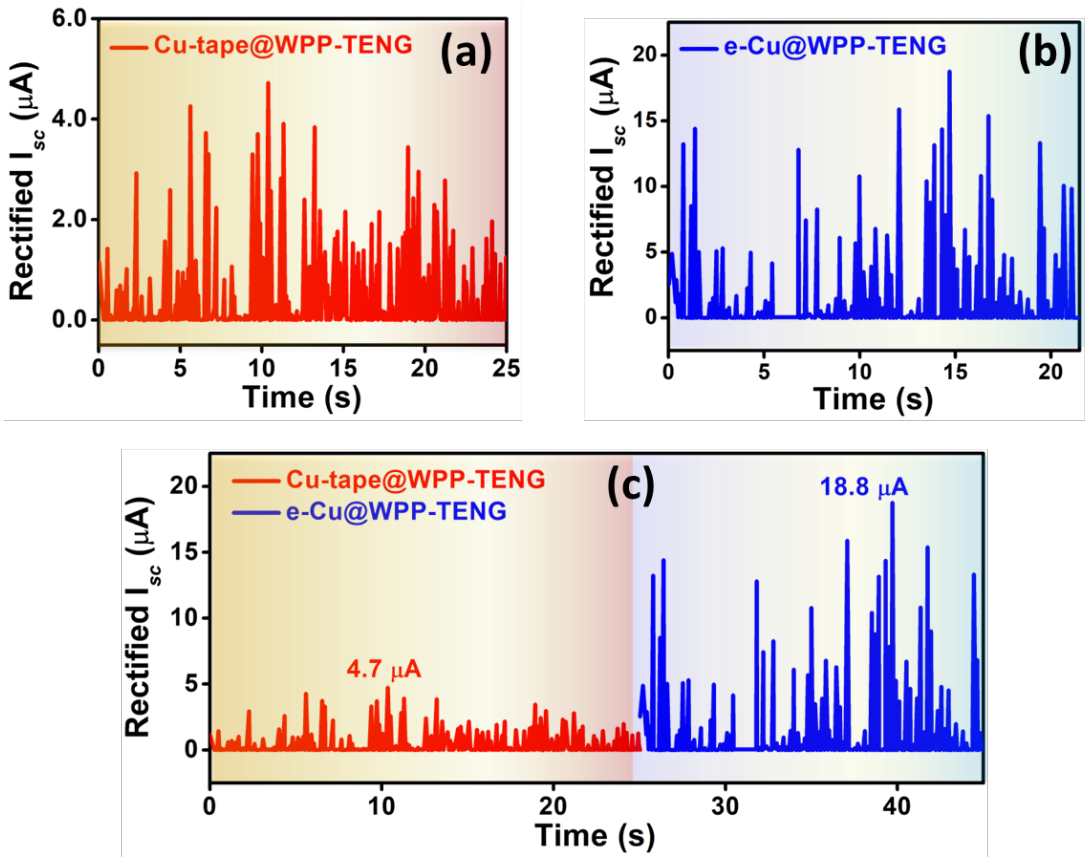

Figure S16. Individual rectified short-circuit current response of (a) Cu-tape@WPP-TENG and (b) e-Cu@WPP-TENG, (c) comparison of current response for Cu-tape@WPP-TENG and e-Cu@WPP-TENG.

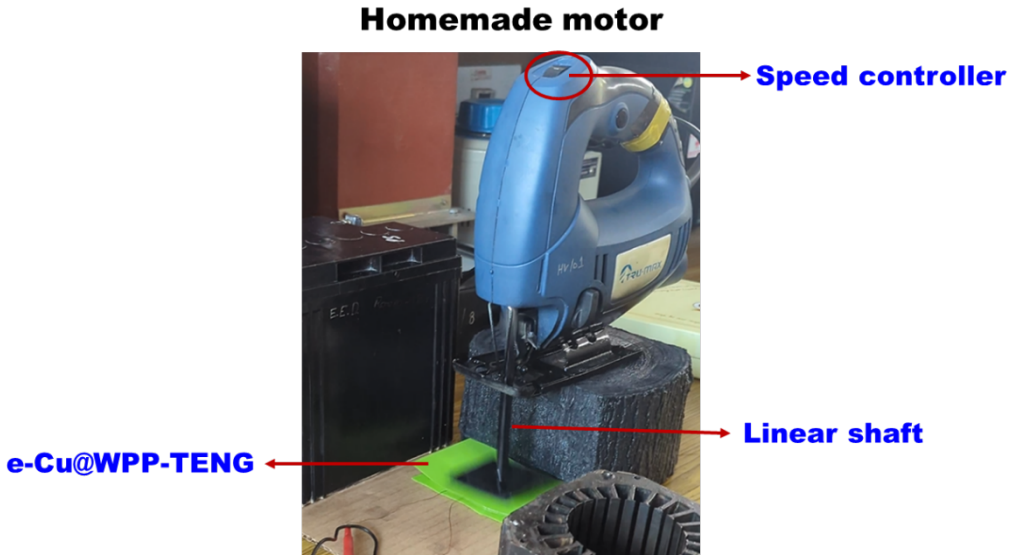

Figure S17. Digital photograph of homemade machine for vertical contact separation of TENG devices. (Mechanical input by homemade motor: 100 N force, 1100 rpm speed)

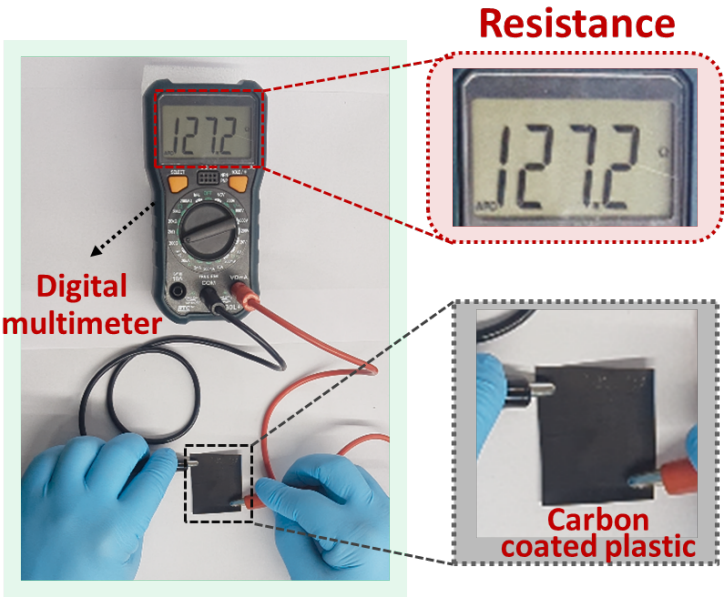

Figure S18. Pictorial representation for the measurement of electrical resistance of carbon-coated plastic sheet by the digital multimeter.

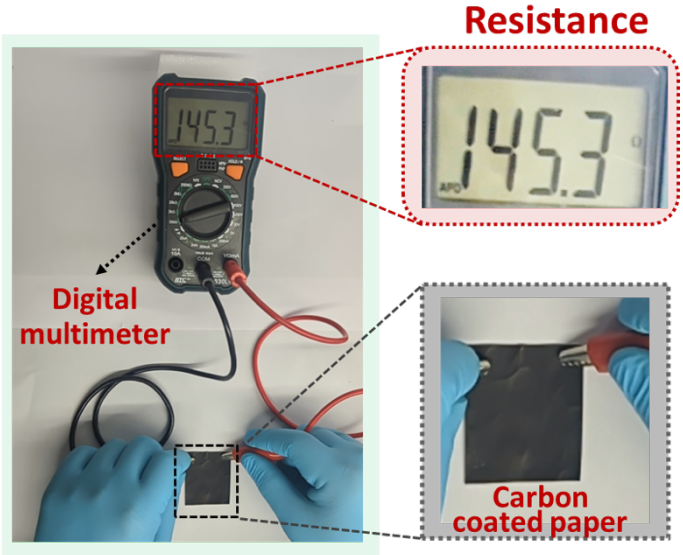

Figure S19. Digital photographs showing the measurement of electrical resistance of carbon-coated paper sheet by the digital multimeter.

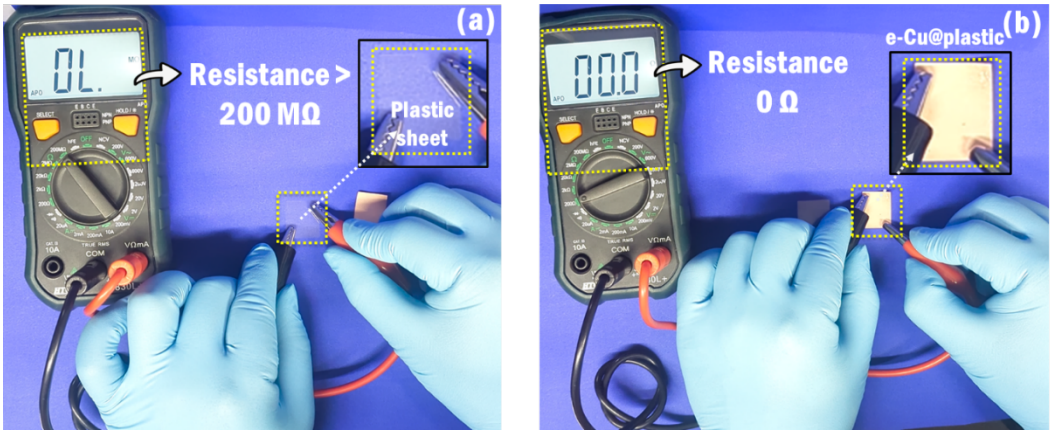

Figure S20. Digital images showing the electrical resistances of (a) plastic sheet, and (b) electrodeposited Cu over plastic sheet.

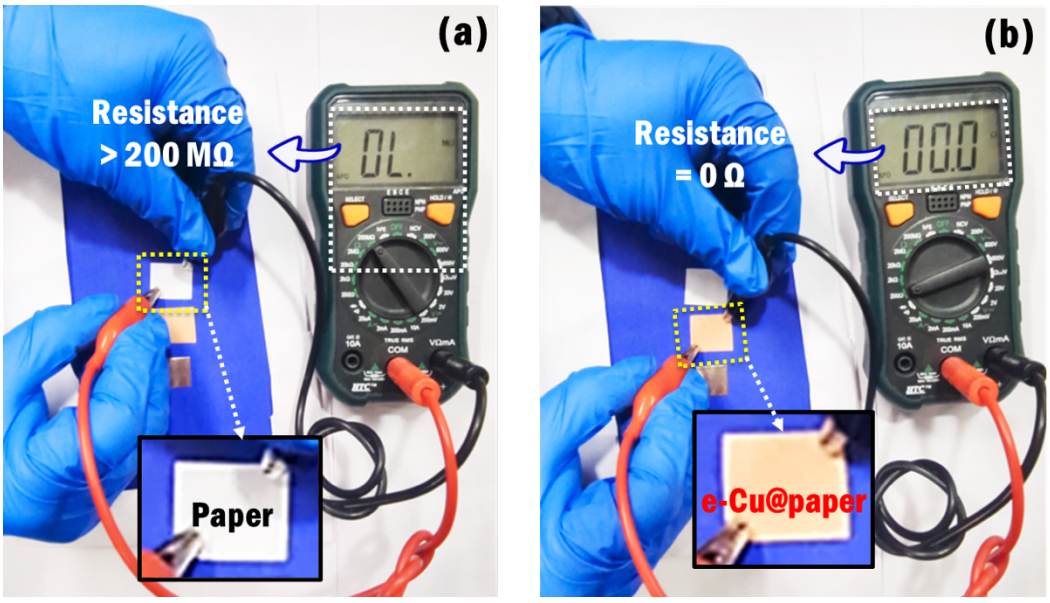

Figure S21. (a) Digital images showing the electrical resistances of (a) paper sheet, and (b) electrodeposited Cu over paper sheet.

Table S1. Literature comparison of various triboelectric nanogenerators made from waste materials.

Sr. no.	Triboelectric materials	Electrode layers	Synthesis method	V_{oc}	I_{sc}	Peak power	References
1.	Waste plastic bags (-ve and +ve),	Au layer	Vacuum sputtering	35.7 V	5.85 µA	152.6 mW m^{-2}	[2]
2.	Plastic bottle (-ve), Paper (+ve)	Graphite ink coated on paper	Drop coating	83.88 V	101 µA	26.54 µW cm^{-2} at 700 kΩ load	[3]
3.	Discarded plastic (-ve) chocolate wrapper (+ve)	Copper and aluminium layers	Adhesive tapes	58 V	0.4 µA	0.027 W m^{-2} at 45 MΩ	[4]
4.	Waste plastic (-ve); Glove, paper, cotton, glass (+ve)	Aluminium	Adhesive tapes	185 V	1.25 µA	8.1 µW cm^{-2} at 500 MΩ.	[5]
5.	Triboelectric bioplastic	Copper and conductive ink	Pasting the conductive ink	130 V	-	1.27 W m^{-2}	[6]
6.	Teflon (-ve), Wood plastic composite (+ve)	Aluminium tape	Adhesive tape	31 V	30 µA	0.107.5 W m^{-2}	[7]
7.	Enzymatic paper (+ve), PVDF (-ve)	Ag tape	Adhesive tape	91.48 V	4.84 µA	0.080.3 W m^{-2}	[8]
8.	PVA-chitosan	Aluminium	Pasting with adhesive	20 V	0.2 µA	0.45 µW at 500 MΩ	[9]
9.	Paper (+ve), Polyimide (-ve)	Laser induced graphene	Laser induced graphene	450 V	5.5 µA	~1.4 mW at 170 MΩ	[10]
10.	Waste polystyrene (+ve), PTFE (-ve)	Al and Cu tapes	Adhesive tapes	300 V	52 µA	4.05 W m^{-2}	[11]
11.	**Waste plastic (-ve), Paper (+ve)**	**Copper**	**Electrode posited Cu**	**552 V**	**18.8 µA (15.6 mA m^{-2})**	**7.68 W m^{-2} or 768 µW cm^{-2} at 1 MΩ load**	**This work**

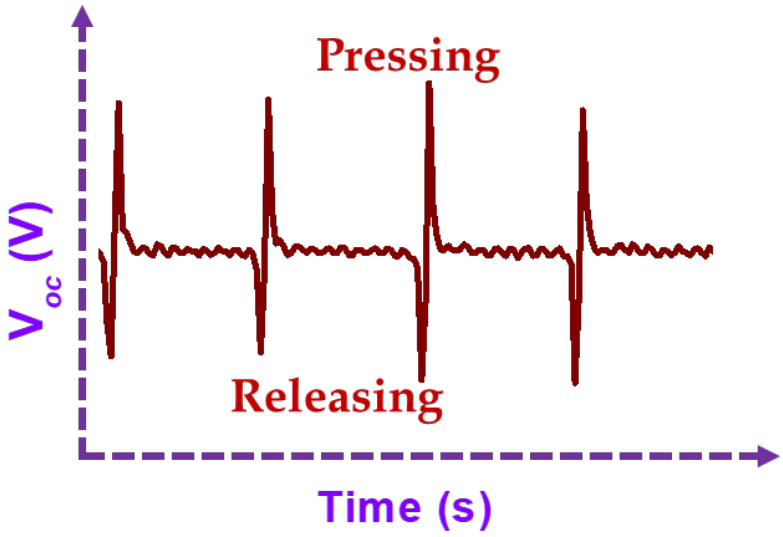

Figure S22. Schematic representation for the signal response of open circuit voltage of e-Cu@WPP-TENG produced by hand pressing.

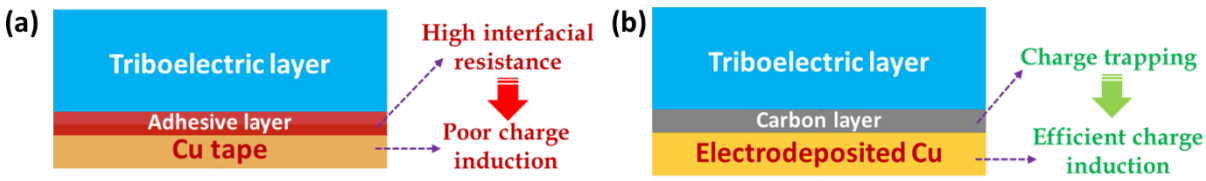

Figure S23. Schematic showcase of different layers of (a) Cu-tape@WPP-TENG & (b) e-Cu@WPP-TENG.

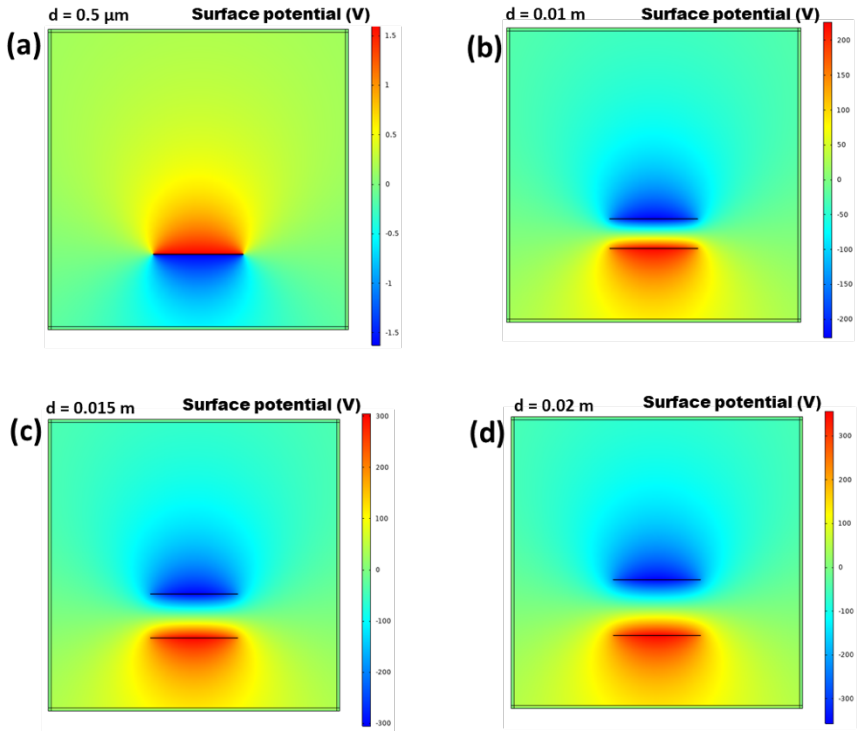

Figure S24. COMSOL simulation results for Cu-tape@WPP-TENG at various separation distance (d = 0 to 20 mm) between the triboelectric layers.

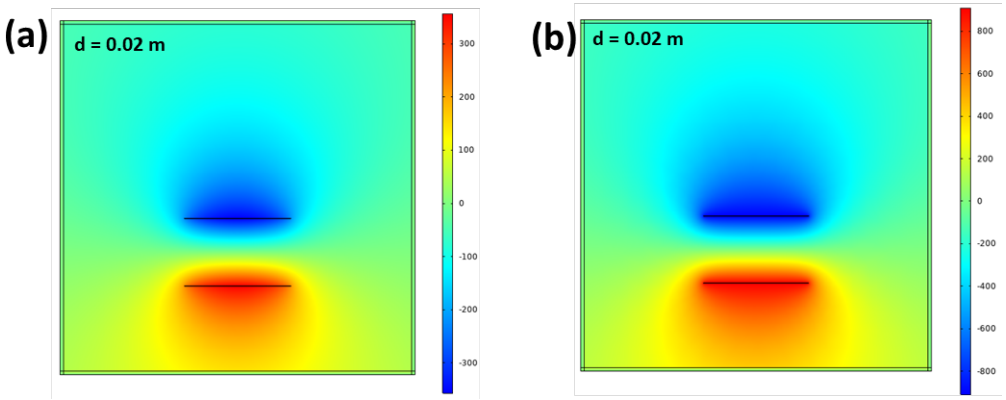

Figure S25 (a-b) Comparison of COMSOL simulation results for Cu-tape@WPP-TENG and e-Cu@WPP-TENG at separation distance of 20 mm between the triboelectric layers

Table S2. Literature comparison of various TENG devices to power the commercial capacitors.

Sr. no.	TENG device	Capacitor	Voltage	Charging time	References
1.	10PAL-20T-CFs/PDMS TENG	10 μF	3.84 V	140 s	[12]
2.	Rubber/wool-based TENG	10 μF	~0.7 V	120 s	[13]
3.	WM-TENG	10 μF	2 V	180 s	[14]
4.	α-Fe_2O_3/PDMS-Human Hair TENG	3.3 μF, 33 μF, 47 μF and 100 μF	2 V	60 s, 420 s, 540 s and 1140 s	[15]
5.	PP TENG	3 μF, 10 μF	1.5 V, ~0.7 V	50 s	[16]
6.	PPP TENG	30 μF	5.3 V	150 s	[17]
7.	AV film-PDMS TENG	10 μF	1.6 V	3048 s	[18]
8.	MOF–TENG	2.2 μF	2 V	55 s	[19]
9.	S-TENG	10 μF	~5.2 V	300 s	[20]
10.	PVC-PVA/FTC TENG	4.7 μF	10 V	94.9 s	[21]
11.	PVA+Fib1:2 TENG	4.7 μF	2 V	60 s	[22]
12.	MF-TENG	2.2	2 V	300 s	[23]
13.	**e-Cu@WPP-TENG**	**1 μF, 2.2 μF, 4.7 μF, 10 μF, 22 μF, 47 μF**	**10 V**	**14 s, 29 s, 56 s, 171 s, 225 s, 645 seconds**	**This work**

Charging of commercial capacitors by hand tapping movements:

Since the nanogenerator produces the energy as long it is subjected to some mechanical stimulation, therefore, it becomes important to store the harvested energy into the energy storage devices so that it can be used later to power the electronic devices. Capacitors are considered suitable equipment to store energy produced from the nanogenerator as they are capable of storing energy at a rapid rate. However, capacitors have high self-discharge and lose the stored charges rapidly. Therefore, it is critical to test the capacitors with different capacitance values to observe the rate of charging and retention of voltage after charging. Herein, we have studied the charging of six different capacitors with capacitance ratings of 1 μF, 2.2 μF, 4.7 μF, 10 μF, 22 μF and 47 μF by the hand pressing of e-Cu@WPP-TENG. Each capacitor was charged for 10 s and then rested for 120 s. This cycle was repeated 2 to 3 times and voltage at the end of this procedure was observed. 1 μF capacitor was quickly charged to

7 V in the first 10 s however, when charging was stopped its voltage dropped down to 4.1 V after 120 s which was again able to achieve 10 V in the next charging cycle before dropping down to 5.2 V at the end of 2nd rest period. Overall, it retained ~58% and 52% of the voltage stored in the first and second tapping cycles respectively thus having an average voltage retention of 55% after 260 s (Figure S26a). Similarly, 2.2 µF, 4.7 µF, 10 µF, 22 µF and 47 µF capacitors showed average retention of 73%, 77%, 86%, 89% and 90% respectively at the end of ~400 s (Figure 5e & S26 (b-e)). As the capacitance rating increased the ability to hold stored charge increased however the voltage of the capacitor significantly decreased.

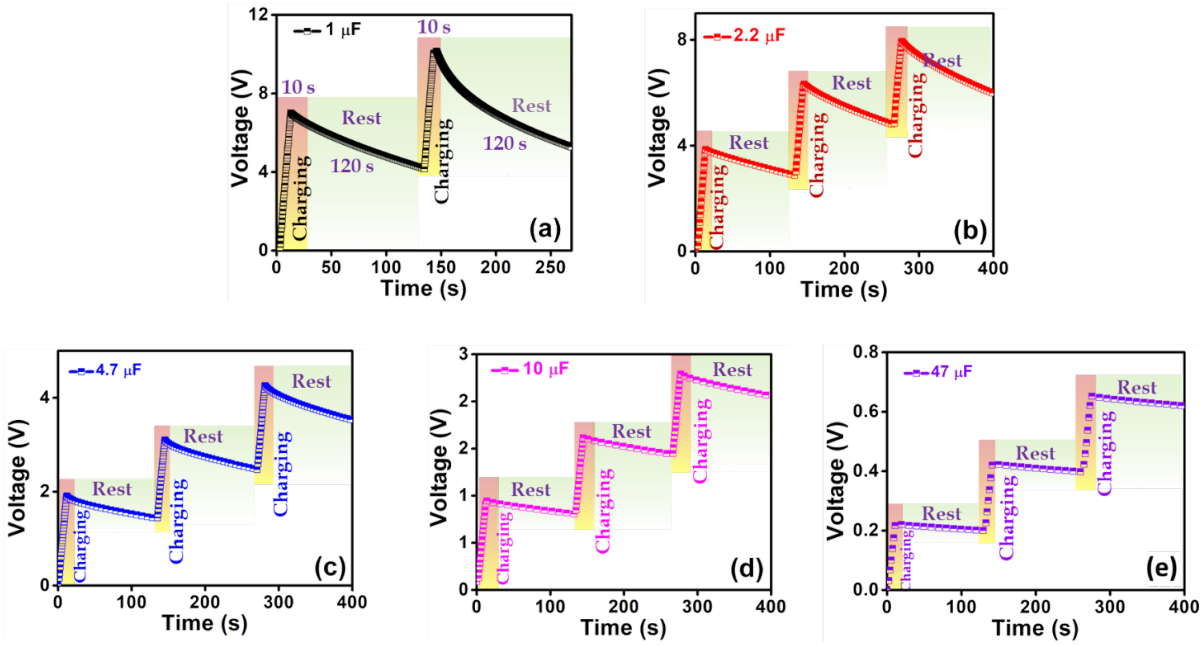

Figure S26. Voltage *vs.* time plot of capacitors with capacitances (a) 1 µF, (b) 2.2 µF, (c) 4.7 µF, (d) 10 µF, and (e) 47 µF charged by e-Cu@WPP-TENG with alternating hand pressing and rest periods of 10 s and 120 s respectively.

The 22 µF capacitor showed fairly good retention of 89% of the stored voltage and e-Cu@WPP-TENG can charge it to ~3.4 V within 1 minute which is sufficient to power most electronic devices such as digital calculators, LCDs etc (Figure 5d). Therefore, 22 µF capacitor was utilized in the electric circuit for the demonstration of powering electronic devices by the TENG.

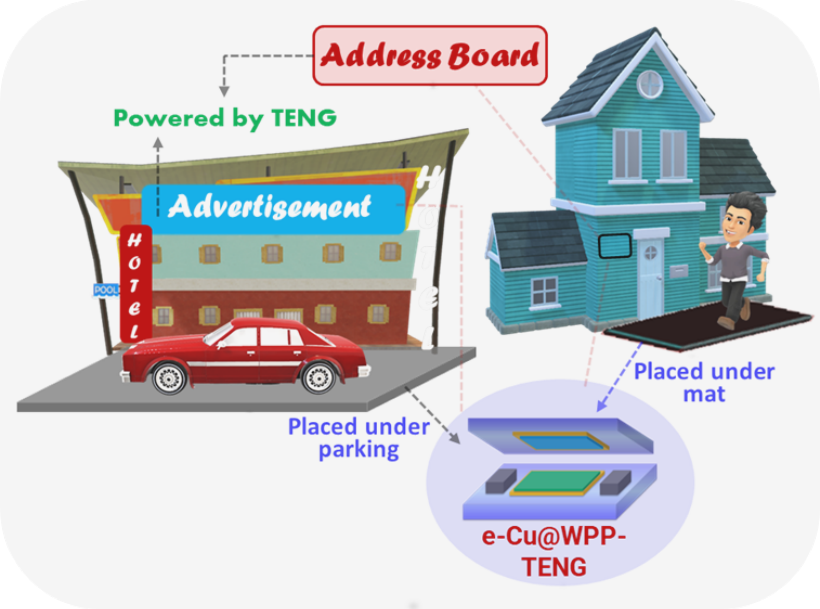

Figure S27. Schematic representation for the practical application of e-Cu@WPP-TENG for powering the LED panels of advertisement, address boards, signs, and name plates, etc.

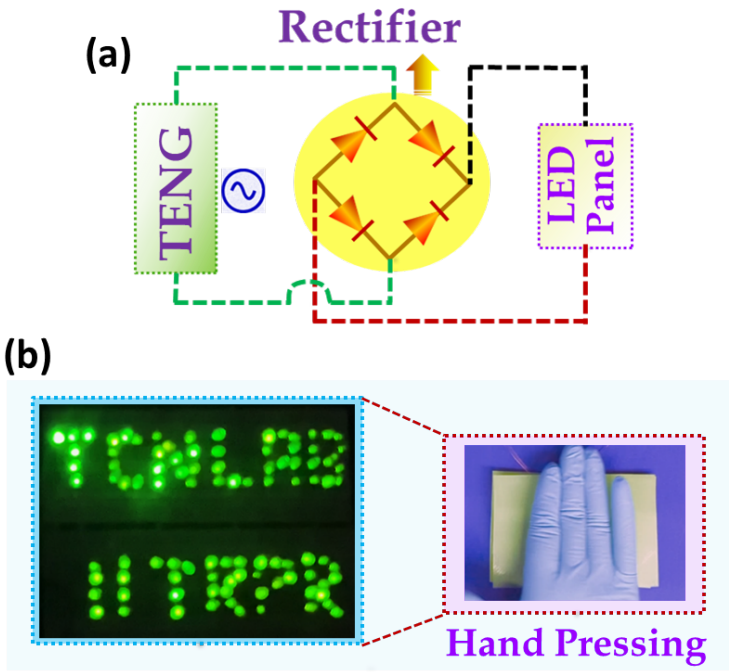

Figure S28. (a) Circuit diagram for powering the LED panel by e-Cu@WPP-TENG, (b) digital photograph showing the laboratory sign board powered by the hand pressing of e-Cu@WPP-TENG.

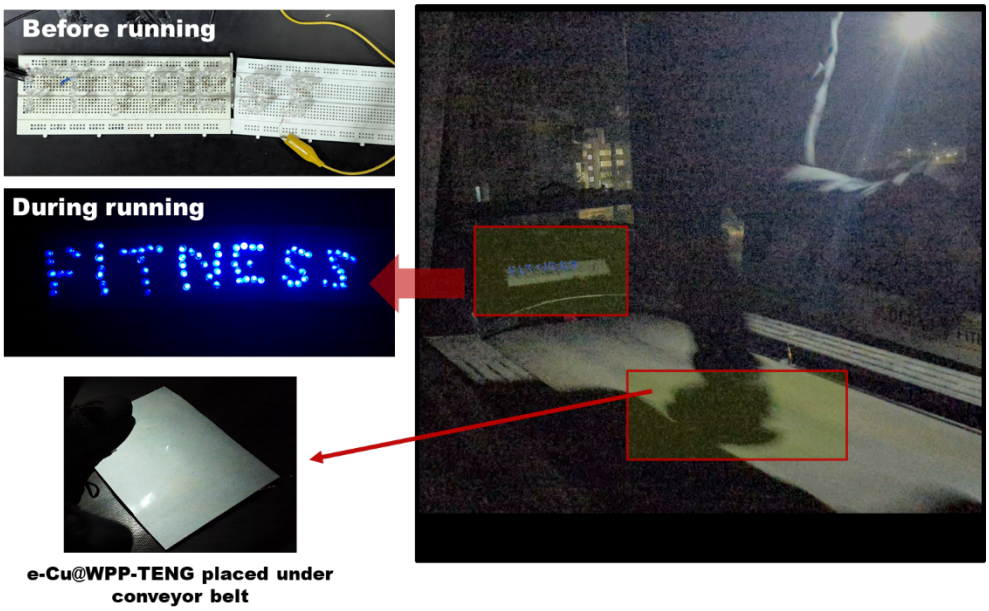

Figure S29. Demonstration of energy harvesting by the running movements of an athlete over the treadmill.

References:

1. B. Abderrahim, E. Abderrahman, A. Mohamed, T. Fatima, T. Abdesselam and O. J. W. J. E. E. Krim, *World J. Environ. Eng.*, 2015, **3**, 95-110.
2. X. Feng, Q. Li and K. Wang, *ACS Appl. Mater. Interfaces*, 2021, **13**, 400-410.
3. M. U. Bukhari, A. Khan, K. Q. Maqbool, A. Arshad, K. Riaz and A. Bermak, *Energy Reports*, 2022, **8**, 1687-1695.
4. N. Kumar Das and S. Badhulika, *Chem. Eng. J.*, 2024, **480**, 147897.
5. M. Sahu, S. Hajra, H.-G. Kim, H.-G. Rubahn, Y. Kumar Mishra and H. J. Kim, *Nano Energy*, 2021, **88**, 106255.
6. Y. Shao, G. Du, B. Luo, T. Liu, J. Zhao, S. Zhang, J. Wang, M. Chi, C. Cai, Y. Liu, X. Meng, Z. Liu, S. Wang and S. Nie, *Adv. Mater.*, 2024, **n/a**, 2311993.
7. V. L. Sunitha, P. Supraja, K. A. K. D. Prasad, M. Navaneeth, A. Babu, V. Mahesh, K. U. Kumar, D. Haranath and R. R. Kumar, *Mater. Lett.*, 2023, **351**, 134995.
8. J. Du, C. Jiao, C. Li, Y. Tao, J. Lu, Y. Cheng, X. Xia, M. Tan and H. Wang, *Nano Energy*, 2023, **116**, 108803.
9. S. Panda, S. Hajra, H.-G. Kim, P. G. R. Achary, P. Pakawanit, Y. Yang, Y. K. Mishra and H. J. Kim, *ACS Appl. Mater. Interfaces*, 2023, **15**, 36096-36106.

10. J. T. Li, M. G. Stanford, W. Chen, S. E. Presutti and J. M. Tour, *ACS Nano*, 2020, **14**, 7911-7919.
11. S. M. Nawaz, M. Saha, N. Sepay and A. Mallik, *Nano Energy*, 2022, **104**, 107902.
12. S. Roy, T. Das, B. Dasgupta Ghosh, K. L. Goh, K. Sharma and Y.-W. Chang, *ACS Appl. Mater. Interfaces*, 2022, **14**, 31973-31985.
13. M. Sahu, S. Hajra, S. Panda, M. Rajaitha, B. K. Panigrahi, H.-G. Rubahn, Y. K. Mishra and H. J. Kim, *Nano Energy*, 2022, **97**, 107208.
14. H. Varghese and A. Chandran, *ACS Appl. Mater. Interfaces*, 2021, **13**, 51132-51140.
15. I. Chakraborty, S.-N. Lai, M.-C. Wu, H.-Y. Lin, C. Li, J. M. Wu and C.-S. Lai, *Mater. Horiz.*, 2021, **8**, 3149-3162.
16. D. Shen, M. Xiao, X. Zhao, Y. Xiao, W. W. Duley and Y. N. Zhou, *ACS Appl. Mater. Interfaces*, 2021, **13**, 34266-34273.
17. S. Roy, P. K. Maji and K.-L. Goh, *Chem. Eng. J.*, 2021, **413**, 127409.
18. N. R. Alluri, N. P. Maria Joseph Raj, G. Khandelwal, V. Vivekananthan and S.-J. Kim, *Nano Energy*, 2020, **73**, 104767.
19. G. Khandelwal, A. Chandrasekhar, N. P. Maria Joseph Raj and S.-J. Kim, *Adv. Energy Mater.*, 2019, **9**, 1803581.
20. H. Patnam, S. A. Graham, P. Manchi, M. V. Paranjape and J. S. Yu, *ACS Appl. Mater. Interfaces*, 2023, **15**, 16768-16777.
21. L. Shi, V. S. Kale, Z. Tian, X. Xu, Y. Lei, S. Kandambeth, Y. Wang, P. T. Parvatkar, O. Shekhah, M. Eddaoudi and H. N. Alshareef, *Adv. Funct. Mater.*, 2023, **33**, 2212891.
22. I. C. M. Candido, G. d. S. Oliveira, S. J. L. Ribeiro, M. Cavicchioli, H. S. Barud, L. G. Silva and H. P. de Oliveira, *Nano Energy*, 2023, **105**, 108035.
23. D. Yang, Y. Ni, X. Kong, S. Li, X. Chen, L. Zhang and Z. L. Wang, *ACS Nano*, 2021, **15**, 14653-14661.